Effects of transforming growth factor-β3 and matrix metalloproteinase-3 on the pathogenesis of chronic mitral valvular disease in dogs

Koji Obayashi, DVM; Sachiko Miyagawa-Tomita, DVM, PhD; Hirotaka Matsumoto, DVM, PhD; Hidekazu Koyama, DVM, PhD; Toshio Nakanishi, MD, PhD; Hisashi Hirose, DVM, PhD

Objective—To investigate the roles of transforming growth factor-β (TGF-β) isoforms and matrix metalloproteinases (MMPs) in development of chronic mitral valvular disease (CMVD) in dogs.

Sample Population—12 mitral valve leaflets collected from cadavers of 5 clinically normal dogs and from 7 dogs with CMVD.

Procedures—Expression of TGF-β isoforms 1, 2, and 3; MMPs 1, 2, 3, and 9; TGF-β receptor II (TβR-II); and α smooth muscle actin (αSMA) in mitral valves of dogs with CMVD was compared with that in mitral valves from clinically normal dogs. Additionally, responses of valvular interstitial cells (VICs) to TGF-β3, MMP-3, and angiotensin-converting enzyme inhibitor (ACEI) as a suppressor of TGF-β3 were examined in vitro.

Results—Expression of TGF-β3, TβR-II, αSMA, and MMP-3 was only detected in mitral valves of dogs with CMVD. Concentrations of αSMA and proteoglycans in cultured VICs were significantly increased following incubation with TGF-β3; treatment with MMP-3 resulted in increased amounts of active and total TGF-β3, and total TGF-β3 in VICs was significantly decreased by incubation with ACEI.

Conclusions and Clinical Relevance—Findings suggested that increased TGF-β3 and MMP-3 contribute to the pathogenesis of valvular degeneration associated with CMVD. In addition, it is possible that the use of ACEI could effectively block pathological alterations in VICs associated with CMVD in vitro.

Impact on Human Medicine—CMVD is associated with primary mitral valve prolapse and Marfan syndrome in humans. Results of the study reported here will help to elucidate the molecular mechanisms of CMVD in dogs and humans. (*Am J Vet Res* 2011;72:194–202).

Chronic mitral valvular disease, also known as myxomatous mitral valve disease, is one of the most commonly acquired cardiovascular diseases in geriatric dogs and is a major cause of morbidity and early death in this species.[1,2] The pathophysiologic changes associated with CMVD cause the mitral valve leaflets to become abnormally thickened, and subsequent malfunction of the mitral valve results in mitral regurgitation. This disease is caused by valvular degeneration and is also characterized by disruption of the collagen and elastin matrix architecture and accumulation of proteoglycans in the spongiosa.[3–5]

The causes and molecular mechanisms of these pathological processes are unknown. However, mechanical stress[6] to the valvular endothelium, VICs, or both has been proposed to lead to pathological transformation of VICs and also to the release of mediators that affect production of proteoglycans and reduction

Abbreviations

ACEI	Angiotensin-converting enzyme inhibitor
αSMA	α Smooth muscle actin
CMVD	Chronic mitral valvular disease
ECM	Extracellular matrix
MMP	Matrix metalloproteinase
p-SMAD2	Phosphorylated Sma and Mad protein 2
TβR-I	Transforming growth factor β receptor I
TβR-I ALK5	Transforming growth factor β receptor I activin receptor-like kinase 5
TβR-II	Transforming growth factor β receptor II
TGF-β	Transforming growth factor β
VIC	Valvular interstitial cell

Received September 3, 2009.
Accepted December 8, 2009.
From the Department of Veterinary Internal Medicine, Faculty of Veterinary Medicine, Nippon Veterinary and Life Science University, 1-7-1 Kyonan-cho, Musashino-shi, Tokyo 180-8602, Japan (Obayashi, Matsumoto, Koyama, Hirose); the Department of Pediatric Cardiology, Heart Institute, Tokyo Women's Medical University, 8-1 Kawada-cho, Shinjuku-ku, Tokyo 162-8666, Japan (Obayashi, Miyagawa-Tomita, Nakanishi); and the Division of Cardiovascular Development and Differentiation, Medical Research Institute, Tokyo Women's Medical University (Miyagawa-Tomita).
Dr. Miyagawa-Tomita was supported in part by Grant-in-Aid for Scientific Research (C).
The authors thank Dr. Koji Tanizawa for providing materials.
Address correspondence to Dr. Miyagawa-Tomita (ptomita@hij.twmu.ac.jp).

of collagen. Several reports[6–10] have suggested that a pathological alteration in VICs is necessary for the development of valvular degeneration. Endothelin,[11–13] nitric oxide,[14] MMPs[6,9,15] and TGF-β isoforms[16] are among the proposed potential mediators; however, the precise contribution of these and other potential mediators of valvular degeneration remains unclear.

Chronic mitral valvular disease in dogs is similar to mitral valve prolapse and to the valvular diseases associated with Marfan syndrome in humans. Studies of mice with phenotypes of mitral valve prolapse[17] and with features of Marfan syndrome[18] strongly suggested that enhanced MMP-2 or TGF-β signaling may be related to the pathogenesis of mitral valve prolapse.

Members of the MMP family of zinc-dependent endoproteases play important roles in ECM degradation in many tissues, including cardiac valves.[19] The TGF-β family of ligands and receptors includes TGF-β, bone morphogenetic proteins, activins, and inhibins. Three major isoforms of TGF-β, designated TGF-β1, TGF-β2, and TGF-β3, are produced in multiple cell types and participate in a wide array of cellular responses including proliferation, differentiation, inflammation, ECM deposition, and apotosis.[20] The TGF-β isoforms are synthesized as prepropolypeptides that are proteolytically processed in the Golgi apparatus to a mature growth factor and its propeptide, also known as latency-associated peptide. Dimers of mature TGF-β and latency-associated peptide form a tight complex, termed the small latency complex, which is biologically inactive. The small latency complex is covalently bound to another protein called latent TGF-β binding protein, forming a large latency complex. The large latency complex is secreted from cells to the extracellular space, where it binds to the ECM. Several inducers of TGF-β activation have been proposed, including proteolytic enzymes (such as MMPs), the matricellular protein thrombospondin-1, integrins, and ionizing radiation.[20–24]

Although some reports have suggested that TGF-β and MMPs are related to valvular degeneration,[6,9,16,18,25] to the authors' knowledge, no study has shown how these factors affect progression of valvular degeneration. Furthermore, although ACEI has been used well in clinical settings, the effect of ACEI on valvular degeneration has not been reported. The study reported here was performed to investigate the roles that TGF-β isoforms and MMPs play in the development of CMVD in dogs and to provide further insight into the pathogenesis of CMVD.

Materials and Methods

Animals and tissue collection—Hearts were collected from 12 dogs that died naturally or were euthanized. Each dog had previously undergone a physical examination by a veterinarian at the Hospital for Small Animals at Nippon Veterinary and Life Science University or at a referring clinic. Three dogs underwent radiography, 7 underwent radiography and echocardiography, and 2 underwent neither of these procedures. Cardiothoracic ratio,[26] vertebral heart size,[27] and left atrial-to-aortic root ratio[28] were measured as part of the thoracic radiographic and echocardiographic examinations. Seven of the 12 dogs (various breeds; 2 males and 5 females; median age, 11.7 years) each had a clinical diagnosis of CMVD, and these were classified as the CMVD group. Dogs with CMVD had been treated with benazepril hydrochloride, benazepril hydrochloride plus furosemide, or a combination of these drugs with digoxin until the time of death. Because these dogs were client owned, consent for use of tissues in the study was obtained from owners prior to necropsy. Hearts were removed from the dogs (which died naturally despite medical treatment during hospitalization) within 1 hour of death. The 5 remaining dogs were clinically normal Beagles (2 males and 3 females; median age, 3.8 years) that were used for educational purposes in the veterinary teaching hospital. These dogs were not receiving any medications and were classified as the clinically normal group. These dogs were euthanized for reasons not related to the present study via IV administration of thiopental sodium, and hearts were collected within 30 minutes of death. The study was approved by the Bioethics Committee at Nippon Veterinary and Life Science University.

Gross pathologic and histologic examination—The presence or absence of CMVD was confirmed on gross examination and independently classified according to Whitney criteria,[16,29] as subjectively determined by 2 investigators (KO and HH). Valves and chordae tendineae were considered normal when they had thin translucent leaflets with no nodular thickening. Classification of mild CMVD was determined when valves met the criteria for Whitney type I or II classifications (type I changes were characterized by a few small, discrete areas of opacity or nodules in the area of valvular apposition, and type II changes comprised a subjectively increased number of larger nodules) but the chordae tendineae were not affected. Valves of dogs with moderate CMVD met the criteria for Whitney type III classification; these contained either large nodules or plaque-like deformities, and thickening of the chordae tendineae was detected visually. Valves of dogs considered to have severe CMVD met the criteria for Whitney type IV classification; the valves were contracted and distorted, and the free edges of the leaflets may thus have rolled toward the left atrium. The proximal aspect of the chordae tendineae was thickened, elongated, and sometimes ruptured in dogs with severe CMVD.

Following gross examination, half of the anterior mitral valve leaflets were used for culture of VICs, and the heart with remaining leaflets was fixed in 4% formalin for 24 hours at 25°C. Five-micrometer-thick longitudinal tissue sections were dewaxed in xylene and rehydrated through a graded series of ethanol. Some sections were stained with H&E, Masson trichrome stain, Victoria blue-van Gieson stain, and Alcian blue stain.

Antibodies were obtained from various sources, and all antibodies were diluted in blocking solution (PBSS supplemented with 10% normal goat serum). Some sections were pretreated with PBSS supplemented with 0.3% hydrogen peroxide to inhibit endogenous peroxidase activity, incubated in blocking solution, and then incubated with primary antibodies (each diluted 1:400) at 4°C overnight, which included mouse anti-porcine vimentin[a]; rabbit anti-chicken desmin[b]; rabbit anti-human TGF-β1,[c] TGF-β2,[c] TGF-β3,[c] TβR-II,[d]

TβR-I ALK5,[c] MMP-1,[c] and MMP-3[c]; and goat anti-human MMP-2[c] and MMP-9.[c] Sections were also incubated with mouse anti-human αSMA[f] (diluted 1:1,000). Secondary antibodies (biotinylated anti-mouse IgG,[g] anti-rabbit IgG,[g] or anti-goat IgG[g] [each diluted 1:200]) were applied to the sections for 30 minutes at 25°C according to the source of primary antibodies. Immunoreactivities were detected by use of a peroxidase-labeled avidin-biotin complex kit,[h] and peroxidase activity was detected by use of 3,3′-diaminobenzidine tetrahydrochloride[i] as a chromagen substrate. Sections were counterstained with hematoxylin. To create negative control tissue sections, the primary antibody was replaced with mouse IgG,[g] rabbit IgG,[j] or goat IgG.[k] For positive control tissues, chick embryonic and canine heart sections (obtained in our laboratory from unrelated experiments) were used.

Culture and immunostaining of VICs—For in vitro culture of VICs,[30] anterior mitral valve leaflets collected from the 5 clinically normal dogs were excised one-third of the distance from the base of the cusp. The leaflets were washed in PBSS on ice and then minced into small pieces. The pieces (1 to 2 mm^2) were plated and cultured (37°C, 5% CO_2, and 100% humidity) in Iscove modified Dulbecco medium[l] supplemented with 10% fetal bovine serum[m] and 1% antibiotic-antimycotic.[l] According to the method of Pho et al,[30] collected cells were split 1:3 at 70% confluence and the cells from passages 3 to 5 were used to seed cultures for each experiment. Primary antibodies against TGF-β1, TGF-β2, TGF-β3, TβR-II, MMP-3, αSMA, desmin, vimentin (all diluted as described for tissue sections), and mouse anti-human CD31[n] (diluted 1:200) were used to test cultured cells. The latter 3 antibodies were used as markers of myocardial, mesenchymal, and endothelial cells, respectively.

The VICs were seeded at 5×10^3 cells/cm^2 and were maintained in complete culture medium as previously described (the day of seeding was considered day 0). After 3 days and at approximately 70% confluence, the cells were immunostained[30] in culture plates. The cells were rinsed once with PBSS and fixed for 10 minutes in 4% paraformaldehyde in PBSS at 25°C. Cells were permeabilized with PBSS supplemented with 0.1% nonionic surfactant solution,[o] incubated with blocking solution for 1 hour, and then incubated with primary antibodies at 4°C overnight. The cells were incubated with the previously described biotinylated secondary antibodies for 30 minutes at 25°C and then incubated with fluorescence-labeled streptavidin solution.[p] Nuclei were counterstained with 4′,6′-diamidino-2-phenylindole. Cells were examined and images were obtained by use of a fluorescence microscope,[q] and the number of cells that were positive for desmin, vimentin, and αSMA were counted; percentages of the total cell count were calculated by dividing the number of positively labeled cells by the number of 4′,6′-diamidino-2-phenylindole–stained cells.

Western blotting—After seeding as described (day 0), cultured VICs were incubated for 3 days with the following treatments in separate wells: goat anti-chicken TGF-β3 neutralizing antibody[r] (5 μg/mL), TGF-β3 peptide[s] (1 ng/mL or 10 ng/mL), or TGF-β3 peptide (1 ng/mL) plus [3-(Pyridin-2-yl)-4-(4-quinonyl)]-1H-pyrazole (a 5μM TβR-I kinase inhibitor).[t] Cultured VICs with no treatment were used as control samples. After 3 days of incubation, cultured VICs were lysed in lysis buffer solution[u] and centrifuged at 12,000 × *g* at 4°C for 15 minutes, and the supernatant was recovered. Protein concentration was measured by use of a protein assay kit,[v] and equal amounts of total protein were separated via SDS-PAGE with 12% Bis-tris–containing polyacrylamide gels[l] and then transferred to polyvinylidene difluoride membranes. The membranes were incubated with the previously described anti-αSMA (diluted 1:1,000), rabbit anti-human p-SMAD2[w] (1:500), and mouse anti-human β actin[e] antibodies (1:2,000), followed by AP-conjugated anti-mouse IgG or anti-rabbit IgG secondary antibodies[x] selected according to the source of the primary antibodies. Blots were developed by use of a chemiluminescent detection system,[x] and bands were detected by use of an image analysis system.[y] The bands were quantified by use of an optional software application supplied with the image analyzer.[y]

Proteoglycans analysis—Proteoglycans were quantified by use of a commercially available mu-

Table 1—Characteristics of 7 dogs with CMVD.

Age (y)	Breed	Sex	Medication	CR (%)	VHS (No. of vertebral lengths)	LA: Ao	Cause of death	Whitney type
14	Pomeranian	F	BNZ, furosemide, digoxin	72.7	12.1	ND	PE	IV
12	Maltese	M	BNZ, furosemide, digoxin	ND	ND	ND	PE	IV
12	Miniature Dachshund	F	BNZ, furosemide, digoxin	77.4	10.4	ND	PE	IV
13	Shi Tzu	F	BNZ, furosemide, digoxin	73.4	11.5	ND	PE	IV
11	Shi Tzu	F	BNZ, furosemide, digoxin	ND	ND	ND	PE	IV
10	Beagle	F	BNZ	67.0	10.4	1.54	Pn	III
10	Beagle	M	BNZ, furosemide	69.0	13.0	1.87	PE	IV

All dogs had previously undergone physical examination; 3 dogs had also undergone only radiography, 2 had undergone radiography and echocardiography, and 2 had undergone neither of these procedures. The cause of death was respiratory insufficiency related to heart failure with pulmonary edema or pneumonia. During postmortem gross examination, mitral valves were evaluated according to Whitney criteria[16,29]; dogs were considered to have moderate or severe CMVD when valves met criteria for Whitney type III or IV classfications, respectively. None of the mitral valves met criteria for Whitney type I or II classifications (ie, mild CMVD).

BNZ = Benazepril hydrochloride. CR = Cardiothoracic ratio. F = Female. LA:Ao = Left-atrial-to-aortic-root ratio. M = Male. ND = Not determined. PE = Pulmonary edema. Pn = Pneumonia. VHS = Vertebral heart size.

copolysaccharide assay kit.[z] The assay was performed according to the manufacturer's instructions. The same treatments were applied to cultured VICs as described for western blot analysis. The VICs were lysed in lysis buffer at 60°C for 1 hour; lysates were combined with reaction buffer, and absorbance at 650 nm was measured via a spectrophotometer.

ELISAs—An ELISA specific for the active human TGF-β3 homodimer[aa] was used to assess the amount of TGF-β3 in VICs incubated with MMP-3, MMP-3 plus an MMP-3 inhibitor, ACEI, or no treatment (as controls) in separate experiments. Cultured cell suspensions were treated according to the manufacturer's instructions; samples were acidified by addition of 1N HCl. After 10 minutes, the sample was neutralized with 1.2N NaOH (to determine the total amount of TGF-β3). Active TGF-β3 was measured in samples prior to acid treatment.

For all ELISAs, microplates were coated with anti–TGF-β3 capture antibody overnight at 25°C and blocked with PBSS supplemented with 1% bovine serum albumin for 1 hour. Samples or standards were added to coated plates, incubated at 25°C for 2 hours, and then aspirated. Each plate was incubated with anti–TGF-β3 detection antibody for 2 hours, followed by incubation with horseradish peroxidase–conjugated streptavidin solution. Color development was achieved by addition of the substrate, and the reaction was allowed to proceed for 20 minutes. When color development was complete, the reaction was stopped by the addition of 2N H_2SO_4 and absorbance at 450 nm was measured via a spectrophotometer.

To assess the effect of MMP-3 on amounts of active and total TGF-β3 in cultured cell suspension (which included VICs and ECM), VICs were treated with recombinant human MMP-3[bb] (30 ng/mL; activated before use via incubation with 4-aminophenylmercuric acetate[f] at 37°C for 20 hours) or with the MMP-3 treatment combined with 4-(4′-Biphenyl)-4-hydroxyiminobutyric acid MMP-3 inhibitor[cc] at 37°C for 1 hour.

To assess the effect of ACEI on TGF-β3 synthesis in VICs, the VICs were incubated with an ACEI[dd] (2mM) for 3 days. The total TGF-β3 concentration in the cell suspension was measured.

Statistical analysis—Results are expressed as the mean ± SD for 3 independent experiments. A statistical analysis was performed by use of a 2-tailed Mann-Whitney *U* test or by use of ANOVA with a Student-Newman-Keuls test. Results were considered to be statistically significant for values

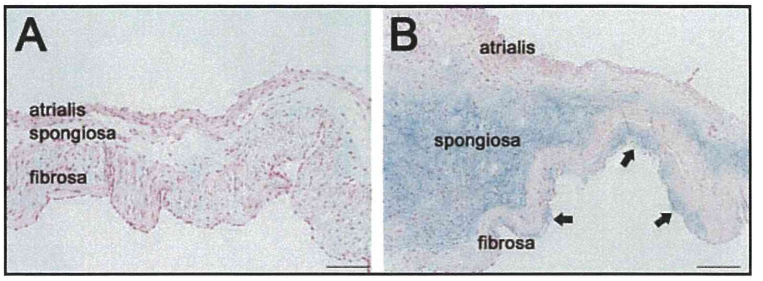

Figure 1—Representative photomicrographs of longitudinal sections of anterior mitral valves from a clinically normal dog (A) and a dog with moderate CMVD (B). In panel A, the normal mitral valve has 3 well-defined tissue layers: atrialis, spongiosa, and fibrosa. In panel B, the mitral valve from a dog with CMVD has an abnormally layered architecture with an expanded spongiosa strongly positive for proteoglycans (blue), loose collagen and accumulation of proteoglycans (arrows) in the fibrosa, and disrupted elastin in the atrialis. The distal aspect of the valve leaflet is on the left. The proximal aspect of the valve leaflet is on the right. Alcian blue stain; the bar in panel A represents 100 μm, and the bar in panel B represents 200 μm.

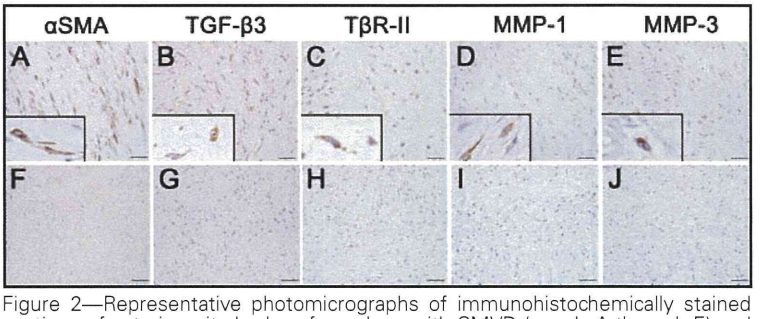

Figure 2—Representative photomicrographs of immunohistochemically stained sections of anterior mitral valves from dogs with CMVD (panels A through E) and from clinically normal dogs (F through J). Expression of αSMA (panels A and F), TGF-β3 (B and G), TβR-II (C and H), and MMP-3 (E and J) was detected in VICs of all dogs with CMVD, but was not detected in those of dogs without CMVD. Expression of MMP-1 was detected in VICs of 3 of 7 dogs with CMVD (panel D), but was not detected in those of clinically normal dogs (I). Positive expression is indicated by brown labeling of cells. Sections were counterstained with hematoxylin. Bars = 50 μm; inset (lower left) of panels in the top row, 600X magnification.

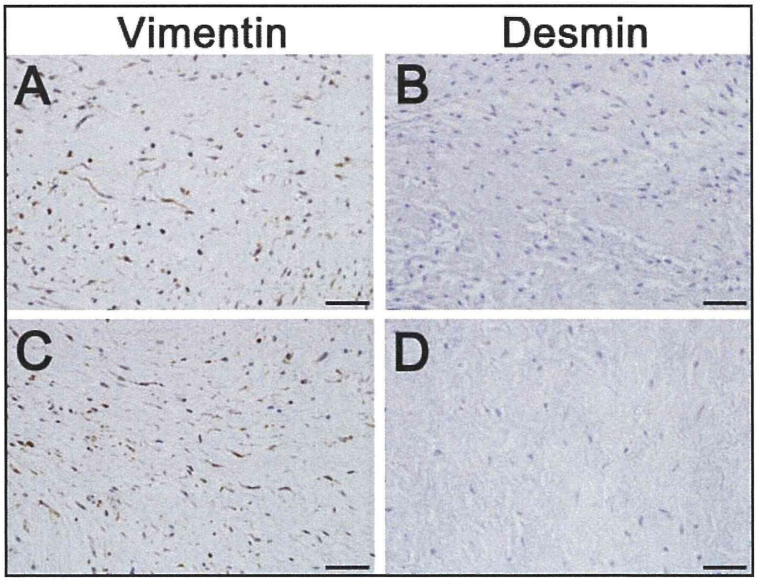

Figure 3—Representative photomicrographs of immunohistochemically stained sections of anterior mitral valves from dogs with CMVD (panels A and B) and from clinically normal dogs (C and D). In mitral valves of dogs of both groups, cytoplasmic expression of vimentin (A and C) but not desmin (B and D) was detected in VICs. *See* Figure 2 for remainder of key.

of $P \leq 0.05$. All analyses were performed by use of a commercially available statistical software program.[ee]

Results

Clinical findings and gross morphology of the heart—The mitral valves of the 5 clinically normal dogs were all classified as normal during gross pathological examination. The 7 dogs with CMVD each had a left systolic regurgitant heart murmur of grade 3/6 or higher. Echocardiographic findings of mitral regurgitation (including irregular and thickened mitral valve leaflets) were assessed in 2 dogs with CMVD. Radiographic findings included enlargement of the heart in 5 dogs with CMVD (increased cardiothoracic ratio [mean value, 71.9%; normal ratio, ≤ 65%[26]] and vertebral heart size [mean value, 11.48 vertebral lengths; normal value, 9.7 ± 0.5 vertebral lengths[27]). Cause of death (determined on the basis of physical examination and necropsy findings, which included radiographic analysis for 5/7 dogs, results of a CBC for 2/7 dogs, and results of serum biochemical analysis for 1/7 dogs) was respiratory insufficiency related to heart failure with pulmonary edema or pneumonia. Of the 7 dogs in the CMVD group, gross examination of the hearts revealed that 1 had moderate CMVD and 6 had severe CMVD (**Table 1**).

Histopathology and immunohistochemistry—Histologic findings for anterior mitral valves from clinically normal dogs were compared with those from dogs in the CMVD group (**Figure 1**). The 3 tissue layers of the valves (the atrialis, mainly composed of elastic fibers and few collagen fibers; the centrally located spongiosa, composed of small amounts of proteoglycans; and the fibrosa, predominantly composed of collagen fibers arranged parallel to the free edge of the leaflet) were well-defined in clinically normal dogs, and the surface of these valves was covered by a single layer of endothelial cells. In contrast, anterior mitral valves from dogs in the CMVD group were characterized by multifocal expansion of the valvular layers, predominantly due to increased deposition of proteoglycans in the spongiosa.

In anterior mitral valves of all dogs with CMVD, intracytoplasmic expression of αSMA, TGF-β3, and TβR-II was detected in VICs in the deep regions of the atrialis and spongiosa layers; in contrast, VICs in the valves of clinically normal dogs did not have detectable expression of these factors (**Figure 2**). The VICs in mitral valves of dogs in both groups expressed vimentin, TGF-β1, and TGF-β2 in the cytoplasm and TβR-I ALK5 in the cytoplasm and nucleus, but did not express detectable amounts of desmin (**Figures 3 and 4**).

The VICs in anterior mitral valves from 7 of 7 dogs with CMVD expressed MMP-3 in the cytoplasm, and in 3 of 7 dogs with CMVD, these cells also expressed MMP-1 in the cytoplasm (Figure 2). However, no expression of MMP-2 or MMP-9 was detected in mitral valve VICs of dogs with CMVD (**Figure 5**). No positive expression of MMP-1, MMP-2, MMP-3, or MMP-9 was detected in VICs of mitral valves from clinically normal dogs.

Immunocytochemistry of cultured mitral valve VICs—Cultured VICs from clinically normal dogs were

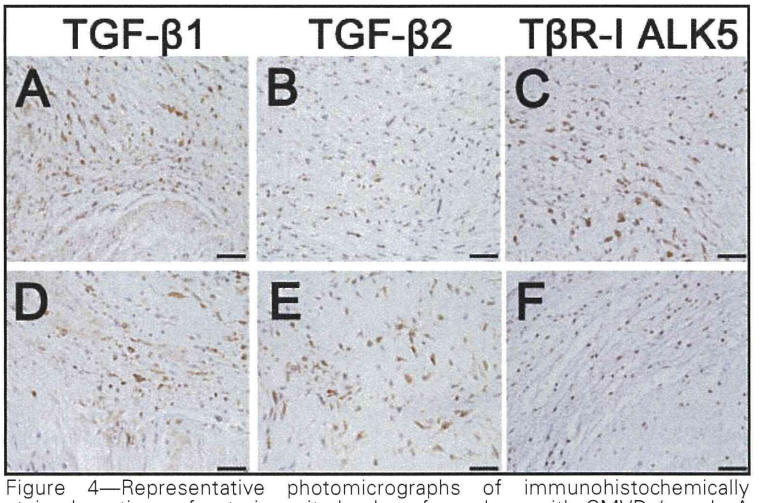

Figure 4—Representative photomicrographs of immunohistochemically stained sections of anterior mitral valves from dogs with CMVD (panels A through C) and from clinically normal dogs (D through F). The mitral valve VICs of dogs of both groups expressed TGF-β1 and TGF-β2 in the cytoplasm and expressed TβR-I ALK5 in cytoplasm and nuclei; TGF-β1 (indicated by light brown labeling) was also expressed in ECM in the spongiosa layer (panels A and D). *See* Figure 2 for key.

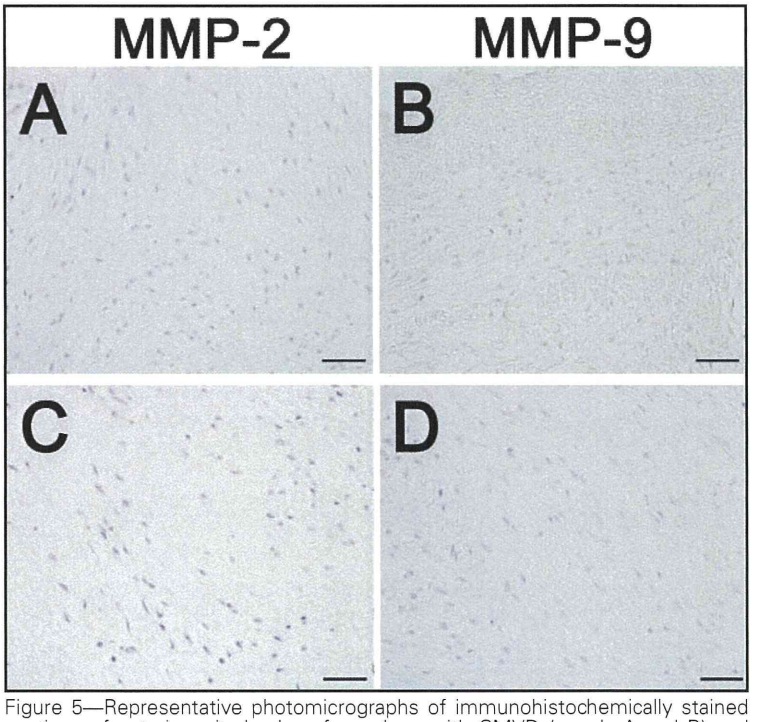

Figure 5—Representative photomicrographs of immunohistochemically stained sections of anterior mitral valves from dogs with CMVD (panels A and B) and from clinically normal dogs (C and D). Expression of MMP-2 or MMP-9 was not detected in the mitral valve VICs of dogs of either group. *See* Figure 2 for key.

confirmed to include no endothelial cells by use of antibodies against the adhesion molecule CD31, and only a small number of cells (≤ 1%) tested positive for the myocardial cell marker desmin (data not shown). The cultured VICs had a spindle-shaped phenotype, and approximately 65% of the cells expressed detectable amounts of αSMA (**Figure 6**). More than 95% of VICs also tested positive for the expression of vimentin (data not shown). The VICs expressed TGF-β2, TGF-β3, TβR-II, and MMP-3 but did not express detectable amounts of TGF-β1. The immunoreactivity patterns in cultured VICs were similar to those detected during histologic analysis of VICs in mitral valves from dogs with CMVD.

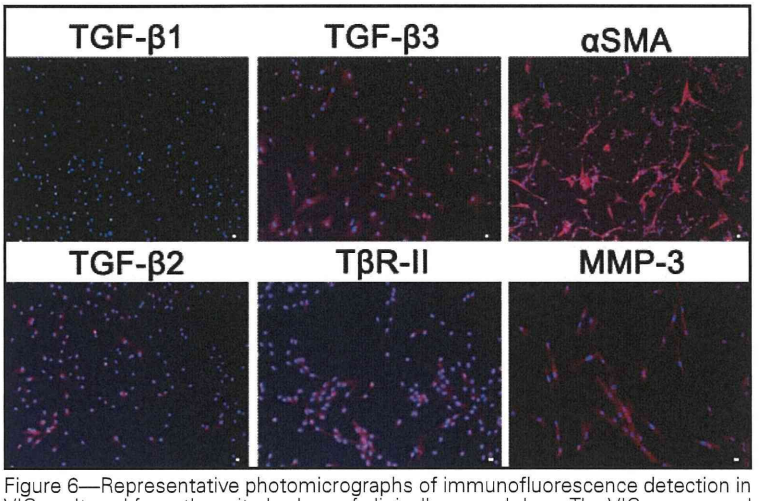

Figure 6—Representative photomicrographs of immunofluorescence detection in VICs cultured from the mitral valves of clinically normal dogs. The VICs expressed TGF-β3, αSMA, TGF-β2, TβR-II, and MMP-3; expression of TGF-β1 was not detected. The immunoreactive patterns detected in cultured VICs resemble those detected in the mitral valve VICs of CMVD-affected dogs via immunohistochemical analysis. Positive result is indicated by red fluorescence; nuclei are counterstained with 4', 6'-diamidino-2-phenylindole (blue fluorescence). Bars = 200 μm.

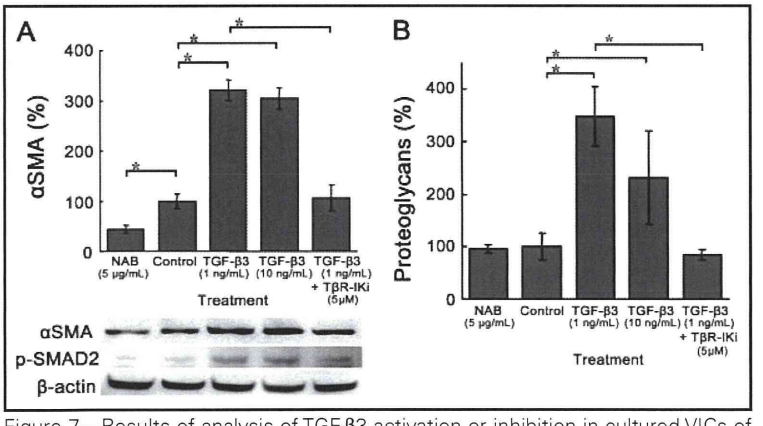

Figure 7—Results of analysis of TGF-β3 activation or inhibition in cultured VICs of clinically normal dogs. Cultured cells were treated with TGF-β3 neutralizing antibody (NAB), no treatment (control), TGF-β3, or TGF-β3 plus TβR-I kinase inhibitor (TβR-IKi). In panel A, western blots of cultured cell lysates were probed with antibodies against αSMA, p-SMAD2, and β-actin; the graph indicates mean ± SD concentrations of αSMA protein normalized to β-actin of the control sample, and photographs of representative blots are displayed. Concentrations of αSMA were significantly decreased by treatment with NAB and were significantly increased by treatment with TGF-β3; this response was significantly inhibited by the addition of TβR-IKi. In panel B, analysis of proteoglycans concentration in lysates of cultured VICs was performed by use of a mucopolysaccaride assay kit. The graph indicates mean ± SD concentrations of proteoglycans relative to the amount of total protein in the control sample. Treatment with TGF-β3 caused a significant increase in VIC proteoglycan synthesis, which was significantly inhibited by the addition of TβR-IKi. *$P < 0.01$.

TGF-β3 activation of cultured VICs and inhibition of TGF-β3—The VICs that were incubated for 3 days with a neutralizing antibody known to recognize the TGF-β3 isoform had significantly ($P < 0.01$) decreased expression of αSMA (mean ± SD, 44 ± 7%; **Figure 7**). Conversely, stimulation with TGF-β3 induced a significant increase in αSMA expression in cultured VICs; the results of analysis of western blots indicated that αSMA expression increased significantly ($P < 0.01$) after treatment with TGF-β3 at concentrations of 1 ng/mL (321 ± 21%) or 10 ng/mL (305 ± 21%) and that this increase was significantly ($P < 0.01$) blocked by treatment with TβR-I kinase inhibitor (106 ± 26%). Expression of p-SMAD2 was increased but was nonsignificant after TGF-β3 treatment. The morphology of VICs was not changed by the culture system or by the described treatments.

Effect of TGF-β3 on proteoglycans synthesis—The addition of TGF-β3 (1 or 10 ng/mL) to VICs in culture for 3 days resulted in significantly ($P < 0.01$) increased synthesis of proteoglycans (348 ± 56% and 231 ± 89%, respectively). Treatment with TβR-I kinase inhibitor significantly ($P < 0.01$) suppressed the effect of TGF-β3 on proteoglycans synthesis (84 ± 10%; Figure 7).

MMP-3 mediated changes in amounts of active and total TGF-β3—The ability of MMP-3 to trigger the release of active and total TGF-β3 from cultured VICs was confirmed via ELISA (**Figure 8**). Treatment with recombinant human MMP-3 caused significant ($P < 0.05$ and $P < 0.01$, respectively) increases in the mean ± SD concentrations of active (untreated control cells, 9.6 ± 4.0 pg/mL; MMP-3 treated cells, 21.3 ± 5.4 pg/mL) and total (untreated control cells, 24.4 ± 7.1 pg/mL; MMP-3 treated cells, 52.9 ± 4.1 pg/mL) TGF-β3 from the cultured VIC layer. Thereafter, the reactions were significantly ($P < 0.05$) inhibited via addition of the MMP-3 inhibitor (mean ± SD concentrations of active and total TGF-β3, 8.3 ± 3.8 pg/mL and 36.0 ± 6.7 pg/mL, respectively). Treatment with 1 ng/mL TGF-β3 had no influence on the total amount of MMP-3 expression from VICs (data not shown).

Effect of ACEI on TGF-β3 expression—The effect of ACEI on TGF-β3 synthesis in VICs was also assessed via ELISA (Figure 8). Treatment with ACEI caused a significant ($P < 0.05$) decrease in the mean ± SD concentrations of total TGF-β3 in cultured VICs (untreated control cells, 33.4 ± 1.5 pg/mL; ACEI-treated cells, 20.3 ± 1.8 pg/mL).

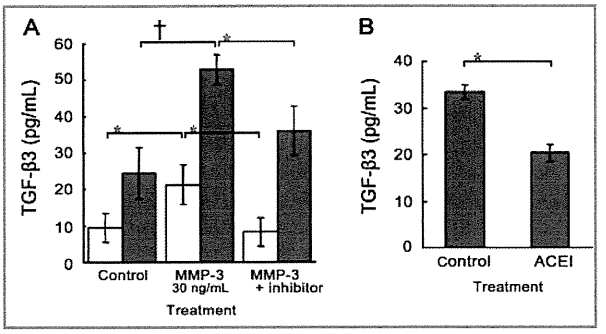

Figure 8—Effects of MMP-3 and ACEI on amounts of active and total TGF-β3 in cultured VICs of clinically normal dogs. In panel A, mean ± SD concentrations of active (white bars) and total (gray bars) TGF-β3 in cultured cells were quantified via ELISA. To determine amounts of active and total TGF-β3, ELISAs were performed before and after acid activation with 1N HCl, respectively. Amounts of active and total TGF-β3 in cultured cells were significantly increased by treatment with recombinant human MMP-3, compared with that of untreated (control) samples; this increase was suppressed by the addition of an MMP-3 inhibitor. In panel B, the total concentration of TGF-β3 in cultured cells was determined via ELISA. Values were significantly decreased by treatment with ACEI, compared with concentrations in control samples. *$P < 0.05$. †$P < 0.01$.

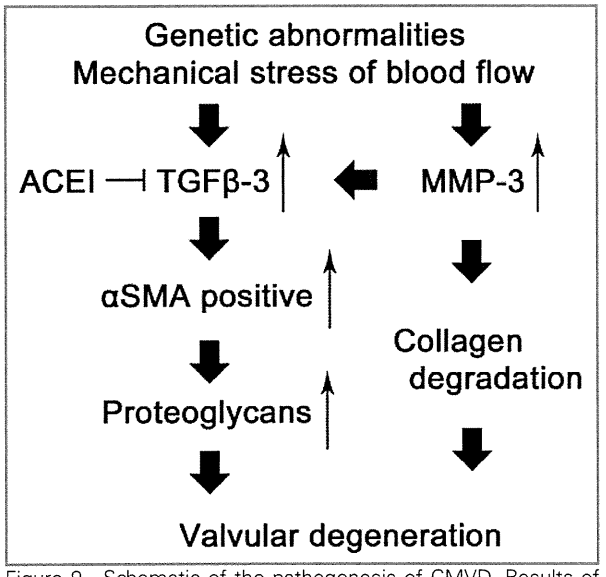

Figure 9—Schematic of the pathogenesis of CMVD. Results of the present study suggested that increased concentrations of TGF-β3 and MMP-3 contribute to the pathogenesis of CMVD and that ACEI may suppress TGF-β3–induced mechanisms of pathogenesis. Thin arrows indicate upregulation. Perpendicular intersecting lines indicate suppression.

Pathogenesis of CMVD—Results of the MMP-3, TGF-β3, and ACEI experiments were used to develop a schematic of the pathogenesis of CMVD in dogs (**Figure 9**). This model incorporated the effects of MMP-3 on TGF-β3 expression and the potential contributions of these factors to the valvular degeneration process.

Discussion

The study reported here demonstrated the roles of TGF-β3 and MMP-3 in the pathogenesis of CMVD in dogs and revealed relationships among TGF-β3, MMP-3, and activated VICs. Nonactivated VICs in healthy cardiac valves have a fibroblast-like morphology, and these cells synthesize collagen, elastin, and proteoglycans. In valves affected by CMVD, degeneration has been mainly detected in the spongiosa layer,[31] and previous reports[6–10] have suggested that phenotypically altered VICs were found in diseased mitral valves; the αSMA-positive cells were characterized as myofibroblasts. In the present study, αSMA positive cells (which are myofibroblasts) were only detected in valves from dogs with CMVD. Therefore, myofibroblasts are considered to play an important role in the pathogenesis of valvular degeneration.

Aupperle et al[16] described the expression patterns of TGF-β isoforms in mitral valves from healthy dogs and from dogs with CMVD, but expression patterns detected in the study reported here were not identical to those findings. The results of the Aupperle et al[16] study indicated increased expression of TGF-β1 and TGF-β3 and weak expression of TGF-β2 in diseased valves. In the present study, however, expression of TGF-β3 and of TβR-II was only detected in the mitral valves of dogs with CMVD, and TGF-β1 and TGF-β2 were equally expressed in mitral valves of clinically normal dogs and dogs with CMVD. These differences may have been attributable to the use of antibodies obtained from different manufacturers, to different fixation times, or to the immunohistochemistry methods that were used.

Although other studies[16,18] indicated that TGF-β1 might play an important role in mitral valve degeneration, results of the present study indicated that mitral valves of clinically normal dogs and of dogs with CMVD equally expressed TGF-β1, whereas TGF-β3 was only expressed in diseased valves. We hypothesized that TGF-β3 and TGF-β1 might cause mitral valvular degeneration in a coordinated manner or that TGF-β3, together with factors other than TGF-β1, might induce this disease. Therefore, we focused particularly on the role of TGF-β3. Little is known about the specific function of TGF-β3; however, TGF-β1, TGF-β2, and TGF-β3 may have distinct functions in the epithelial-mesenchymal transformation that occurs during cardiac valve development.[32] Transforming growth factor-β3 regulates the quality and quantity of ECM and also has a crucial role in atrioventricular valve remodeling in avian species.[33] In the present study, we demonstrated that TGF-β3 singularly regulated valve myofibroblast activation and proteoglycan synthesis in an in vitro system. The modulation attributed to TGF-β3 at least partially involved the p-SMAD2 signaling pathway. The reactions of cultured VICs may not be identical to processes that occur in VICs in vivo because cultured VICs undergo selection processes and stress caused by conditions of the culture itself. In addition, the expression of αSMA has been reported[34] to vary somewhat, depending on the culture period of VICs. A report[6] has also shown that abnormalities of TGF-β3 signaling caused by genetic mutations or mechanical stress may promote pathological ECM remodeling in mitral valves.

The results of some studies[9,15] have also suggested that MMP-1, MMP-2, MMP-13, and MMP-14, as well as tissue inhibitors of metalloproteinase 2 and 3, were expressed in grossly and histologically normal mitral valves of dogs and were involved in ECM metabolism.

Increased expression of MMP-1, MMP-13, and MMP-14 was detected in mitral valves of dogs with CMVD in those studies. In humans, increased expression of MMP-1, MMP-2, MMP-9, and MMP-13 was confirmed in myxomatous heart valves, compared with expression in normal heart valves.[6,25] In the present study, MMP-1 and MMP-3 were only expressed in mitral valves of dogs with CMVD, and MMP-2 and MMP-9 were not expressed in mitral valves of dogs in either group. Expression of MMP-3 in cultured cells of various types was reported to be upregulated in vitro by means of mechanical stimulation, hydrostatic pressure,[35] or stretching.[36] Matrix metalloproteinase-3 degrades a wide range of substrates, including fibronectin; laminin; collagens III, IV, IX, X; and proteoglycans; it also activates pro-MMPs such as pro–MMP-1. It is possible that MMP-3 and MMP-1 may be involved in the destruction of the basal structure of mitral valves.

It is still unclear whether the abnormal accumulation of proteoglycans is a cause or a result of the degradation of ECM. However, the accumulation of proteoglycans may follow the degradation of ECM caused by MMPs.[25] Furthermore, analysis of the results of the study reported here indicated that MMP-3 also increased amounts of active and total TGF-β3. Therefore, MMP-3 and TGF-β3 might contribute to the accumulation of proteoglycans in this tissue.

Treatment with ACEIs has been useful in the management of hypertension and congestive heart disease in humans and dogs. Angiotensin II directly induces the transcription of *Tgfb1* in rats.[37] Analysis of results of the present study indicated that an ACEI effectively suppressed the amount of total TGF-β3 in vitro, which suggests that ACEIs may be useful for the prevention or treatment of CMVD; however, additional experiments should be performed to confirm that the reported effect was caused by prevention of angiotensin II formation in cultured VICs.

The study reported here was limited because the number of dogs was small and almost all of the dogs with a diagnosis of CMVD had clinically severe disease; we were unable to collect samples from dogs that had either mild or early stages of CMVD. We collected tissue specimens from privately owned dogs that had developed CMVD and died naturally. Since most owners cherished their dogs, it was extremely difficult for us to obtain permission to perform postmortem examinations. There were differences in the ages and breeds of dogs between the clinically normal and CMVD groups. The incidence of CMVD has been observed to increase with advancing age. Some studies[38–40] revealed that concentrations of TGF-β isoforms[38,39] and MMPs[40] in human plasma or serum also change with age; as age increased, concentrations of TGF-β1, TGF-β3, and MMP-9 decreased and concentrations of TGF-β2, MMP-2, and MMP-7 increased. Thus, it may be possible that the ages or breeds of the dogs may have affected expression patterns of proteins that were examined in the present study.

Our results indicate that increased TGF-β3 and MMP-3 protein concentrations in mitral valves contribute to the pathogenesis of CMVD in dogs. The factors that regulate TGF-β3 and MMP-3 are still unknown, although it is thought that this regulation involves genetic mechanisms and mechanical stress. Further research is needed to identify new markers for use in the diagnosis of this disease and for the development of new medicines that act on the molecular mechanisms of valvular degeneration.

a. AbD Serotec, Kidlington, Oxfordshire, England.
b. Progen, Land Baden-Württemberg, Germany.
c. Santa Cruz Biotechnology Inc, Santa Cruz, Calif.
d. Upstate Biotechnology, Billerica, Mass.
e. Abcam, Cambridge, England.
f. Sigma-Aldrich Corp, St Louis, Mo.
g. Vector Laboratories Inc, Burlingame, Calif.
h. ABC Elite kit, Vector Laboratories Inc, Burlingame, Calif.
i. Diaminobenzidine, Wako Pure Chemical Industries Ltd, Osaka, Japan.
j. Inter-Cell Technologies Inc, Hopewell, NJ.
k. Chemicon International Inc, Billerica, Mass.
l. Invitrogen Corp, Carlsbad, Calif.
m. Fetal bovine serum, Biowest, Paris, France.
n. DAKO, Glostrup, Denmark.
o. Triton X-100, Wako Pure Chemical Industries Ltd, Osaka, Japan.
p. Streptavidin Hilyte Plus 647 conjugated (60672-Plus647), AnaSpec, Gauteng, South Africa.
q. Fluorescence microscope BZ-8000, Keyence Corp, Osaka, Japan.
r. R&D Systems Inc, Minneapolis, Minn.
s. TGF-β3 peptide (PT-4124), Lonza Group Ltd, Basel-Stadt, Switzerland.
t. TβR-I kinase inhibitor, Calbiochem, Hesse, Germany.
u. CelLytic-M, Sigma-Aldrich Corp, St Louis, Mo.
v. DC protein assay kit, Bio-Rad Laboratories Inc, Hercules, Calif.
w. Signalway Antibody Inc, Pearland, Tex.
x. WesternBreeze chemiluminescent detection system, Invitrogen Corp, Carlsbad, Calif.
y. LAS-3000 UV mini image analysis system with optional software application Multi Gauge software program, version 3.0, FUJIFILM, Tokyo, Japan.
z. Acidic Mucopolysaccaride assay kit, Primary Cell, Hokkaido, Japan.
aa. Active human TGF-β3 homodimer DuoSet ELISA, R&D Systems Inc, Minneapolis, Minn.
bb. Recombinant human MMP-3, AnaspecAnaSpec, Gauteng, South Africa.
cc. MMP-3 Inhibitor VI, Calbiochem, Hesse, Germany.
dd. Enalapril maleate, Sigma-Aldrich Corp, St Louis, Mo.
ee. Ystat 2006, version 5, Igaku Tosho Shuppan, Tokyo, Japan.

References

1. Darke PG. Valvular incompetence in Cavalier King Charles Spaniels. *Vet Rec* 1987;120:365–366.
2. Beardow AW, Buchanan JW. Chronic mitral valve disease in Cavalier King Charles Spaniels: 95 cases (1987–1991). *J Am Vet Med Assoc* 1993;203:1023–1029.
3. Devereux RB. Recent developments in the diagnosis and management of mitral valve prolapse. *Curr Opin Cardiol* 1995;10:107–116.
4. Fontana ME, Sparks EA, Boudoulas H, et al. Mitral valve prolapse and the mitral valve prolapse syndrome. *Curr Probl Cardiol* 1991;16:309–375.
5. King BD, Clark MA, Baba N, et al. "Myxomatous" mitral valves: collagen dissolution as the primary defect. *Circulation* 1982;66:288–296.
6. Rabkin E, Aikawa M, Stone J, et al. Activated interstitial myofibroblasts express catabolic enzymes and mediate matrix remodeling in myxomatous heart valves. *Circulation* 2001;104:2525–2532.
7. Corcoran BM, Black A, Anderson H, et al. Identification of surface morphologic changes in the mitral valve leaflets and chordae tendineae of dogs with myxomatous degeneration. *Am J Vet Res* 2004;65:198–206.
8. Black A, French AT, Dukes-McEwan J, et al. Ultrastructural

morphologic evaluation of the phenotype of valvular interstitial cells in dogs with myxomatous degeneration of the mitral valve. *Am J Vet Res* 2005;66:1408–1414.
9. Disatian S, Ehrhart EJ III, Zimmerman S, et al. Interstitial cells from dogs with naturally occurring myxomatous mitral valve disease undergo phenotype transformation. *J Heart Valve Dis* 2008;17:402–411.
10. Han RI, Black A, Culshaw GJ, et al. Distribution of myofibroblasts, smooth muscle-like cells, macrophages, and mast cells in mitral valve leaflets of dogs with myxomatous mitral valve disease. *Am J Vet Res* 2008;69:763–769.
11. Weber H, Webb ML, Serafino R, et al. Endothelin-1 and angiotensin-II stimulate delayed mitogenesis in cultured rat aortic smooth muscle cells: evidence for common signaling mechanisms. *Mol Endocrinol* 1994;8:148–158.
12. Rizvi MA, Katwa L, Spadone DP, et al. The effects of endothelin-1 on collagen type I and type III synthesis in cultured porcine coronary artery vascular smooth muscle cells. *J Mol Cell Cardiol* 1996;28:243–252.
13. Mow T, Pedersen HD. Increased endothelin-receptor density in myxomatous canine mitral valve leaflets. *J Cardiovasc Pharmacol* 1999;34:254–260.
14. Olsen LH, Mortensen K, Martinussen T, et al. Increased NADPH-diaphorase activity in canine myxomatous mitral valve leaflets. *J Comp Pathol* 2003;129:120–130.
15. Aupperle H, Thielebein J, Kiefer B, et al. An immunohistochemical study of the role of matrix metalloproteinases and their tissue inhibitors in chronic mitral valvular disease (valvular endocardiosis) in dogs. *Vet J* 2009;180:88–94.
16. Aupperle H, Marz I, Thielebein J, et al. Expression of transforming growth factor-beta1, -beta2 and -beta3 in normal and diseased canine mitral valves. *J Comp Pathol* 2008;139:97–107.
17. Mahimkar R, Nguyen A, Mann M, et al. Cardiac transgenic matrix metalloproteinase-2 expression induces myxomatous valve degeneration: a potential model of mitral valve prolapse disease. *Cardiovasc Pathol* 2009;18:253–261.
18. Ng CM, Cheng A, Myers LA, et al. TGF-beta-dependent pathogenesis of mitral valve prolapse in a mouse model of Marfan syndrome. *J Clin Invest* 2004;114:1586–1592.
19. Dreger SA, Taylor PM, Allen SP, et al. Profile and localization of matrix metalloproteinases (MMPs) and their tissue inhibitors (TIMPs) in human heart valves. *J Heart Valve Dis* 2002;11:875–880.
20. Annes J, Munger JS, Rifkin DB. Making sense of latent TGFbeta activation. *J Cell Sci* 2003;116:217–224.
21. Kaartinen V, Warburton D. Fibrillin controls TGF-beta activation. *Nat Genet* 2003;33:331–332.
22. Charbonneau NL, Ono RN, Corson GM, et al. Fine tuning of growth factor signals depends on fibrillin microfibril networks. *Birth Defects Res C Embryo Today* 2004;72:37–50.
23. Ramirez F, Sakai L, Dietz H, et al. Fibrillin microfibrils: multipurpose extracellular networks in organismal physiology. *Physiol Genomics* 2004;19:151–154.
24. Rifkin DB. Latent transforming growth factor-beta (TGF-beta) binding proteins: orchestrators of TGF-beta availability. *J Biol Chem* 2005;280:7409–7412.
25. Togashi M, Tamura K, Nitta T, et al. Role of matrix metalloproteinases and their tissue inhibitor of metalloproteinases in myxomatous change of cardiac floppy valves. *Pathol Int* 2007;57:251–259.
26. Buchanan JW. Patent ductus arteriosus. *Semin Vet Med Surg (Small Anim)* 1994;9:168–176.
27. Buchanan JW, Bücheler J. Vertebral scale system to measure canine heart size in radiographs. *J Am Vet Med Assoc* 1995;206:194–199.
28. Pouchelon JL, Jamet N, Gouni V, et al. Effect of Benazepril on survival and cardiac events in dogs with asymptomatic mitral valve disease: a retrospective study of 141 cases. *J Vet Intern Med* 2008;22:905–914.
29. Whitney JC. Cardiovascular pathology. *J Small Anim Pract* 1967;8:459–465.
30. Pho M, Lee W, Watt DR, et al. Cofilin is a marker of myofibroblast differentiation in cells from porcine aortic cardiac valves. *Am J Physiol Heart Circ Physiol* 2008;294:1767–1778.
31. Tamura K, Fukuda Y, Ishizaki M, et al. Abnormalities in elastic fibers and other connective-tissue components of floppy mitral valve. *Am Heart J* 1995;129:1149–1158.
32. Mercado-Pimentel ME, Runyan RB. Multiple transforming growth factor-beta isoforms and receptors function during epithelial-mesenchymal cell transformation in the embryonic heart. *Cells Tissues Organs* 2007;185:146–156.
33. Norris RA, Potts JD, Yost MJ, et al. Periostin promotes a fibroblastic lineage pathway in atrioventricular valve progenitor cells. *Dev Dyn* 2009;238:1052–1063.
34. Pho M, Lee W, Watt DR, et al. Cofilin is a marker of myofibroblast differentiation in cells from porcine aortic cardiac valves. *Am J Physiol Heart Circ Physiol* 2008;294:H1767–H1778.
35. Neidlinger-Wilke C, Würtz K, Urban JP, et al. Regulation of gene expression in intervertebral disc cells by low and high hydrostatic pressure. *Eur Spine J* 2006;15(suppl 3):S372–S378.
36. Das RH, Jahr H, Verhaar JA, et al. In vitro expansion affects the response of chondrocytes to mechanical stimulation. *Osteoarthritis Cartilage* 2008;16:385–391.
37. Li XC, Zhuo JL. Intracellular ANG II directly induces in vitro transcription of TGF-beta1, MCP-1, and NHE-3 mRNAs in isolated rat renal cortical nuclei via activation of nuclear AT1a receptors. *Am J Physiol Cell Physiol* 2008;294:C1034–C1045.
38. Zhang N, Wu XY, Wu XP, et al. Relationship between age-related serum concentrations of TGF-beta1 and TGF-beta2 and those of osteoprotegerin and leptin in native Chinese women. *Clin Chim Acta* 2009;403:63–69.
39. Hering S, Isken F, Janott J, et al. Analysis of TGF-β3 gene expression and protein levels in human bone and serum. *Exp Clin Endocrinol Diabetes* 2001;109:107–115.
40. Bonnema DD, Webb CS, Pennington WR, et al. Effects of age on plasma matrix metalloproteinases (MMPs) and tissue inhibitor of metalloproteinases (TIMPs). *J Card Fail* 2007;13:530–540.

Pediatr Cardiol (2011) 32:1244–1248
DOI 10.1007/s00246-011-0078-6

CASE REPORT

A Case of Cor Triatriatum With an Abnormal P Wave: The Pacemaker Action From the Specialized Tissue in the Abnormal Septum

Yoshimichi Kudo · Mariko Kaneko · Makoto Nakazawa · Sachiko Tomita

Received: 14 April 2011 / Accepted: 20 July 2011 / Published online: 7 August 2011

Abstract A boy presented with an abnormal P wave shown on an electrocardiogram (ECG) checkup at school. An echocardiogram and contrast-enhanced computed tomography (CT) showed cor triatriatum with a slit-like opening between the accessory chamber and the left atrium located along the interatrial septum. The boy underwent open heart surgery for excision of the anomalous membrane, and a postoperative ECG showed normal P waves. The excised tissue was examined immnunohistopathologically using antihyperpolarization-activated cyclic nucleotide-gated potassium channel 4 (HCN4) antibody and other staining. The authors confirmed the existence of cells positive to HCN4, indicating that they were sinoatrial node cells or at least cells with electrical automaticity.

Keywords ECG checkup · HCN4 · Sinoatrial node cell

Electronic supplementary material The online version of this article (doi:10.1007/s00246-011-0078-6) contains supplementary material, which is available to authorized users.

Y. Kudo (✉) · M. Kaneko
Department of Pediatrics, Southern Tohoku Research Institute for Neuroscience, Southern Tohoku General Hospital, 7-115 Yatsuyamada, Koriyama, Fukushima 963-8563, Japan
e-mail: yoshimichi.kudo@mt.strins.or.jp

M. Nakazawa
Pediatric and Lifelong Congenital Cardiology Institute, Southern Tohoku Research Institute for Neuroscience, Southern Tohoku General Hospital, 7-115 Yatsuyamada, Koriyama, Fukushima 963-8563, Japan

S. Tomita
Department of Pediatric Cardiology, Tokyo Women's Medical University, Tokyo, Japan

Case Report

A 10-year-old boy who was totally asymptomatic and had no congenital heart disease in his family history presented with an abnormal P wave shown in on electrocardiogram (ECG) checkup. He had no abnormal physical findings. His ECG (Fig. 1a) showed large negative P waves in II, III, and aVF and negative P waves in V5 and V6. A chest x-ray was not remarkable, but a questionable double contour was observed, suggesting mild left atrial enlargement.

To exclude any anomalies associated with the abnormal P waves, we performed an echocardiographic examination, which showed an anomalous membrane in the left atrium separating it into two chambers. The one chamber received the pulmonary veins, and the other chamber had the mitral valve, thus leading to the diagnosis of cor triatriatum, classic type as defined in the Moss and Adams' textbook [3]. The opening between the left atrium and the accessory chamber was slit-like and located along the interatrial septum. Its long axis measured 7 mm (Fig. 2). No obvious deviation of the anomalous membrane toward the proper left atrium was observed, indicating that there was no significant hemodynamic obstruction due to the membrane at the time. However, all the pulmonary veins appeared to be somewhat dilated, indicating a subtle and mild pulmonary congestion.

A contrast-enhanced CT confirmed the presence of the opening resembling a slit adjacent to the interatrial septum and close to the posterior wall (Fig. 3). Cardiac catheterization showed no pulmonary hypertension and a pulmonary artery wedge pressure of 12 mm Hg, which was the upper limit of normal.

We had previously experienced another teenager who was completely asymptomatic but became severely ill from acute pulmonary congestion immediately after a

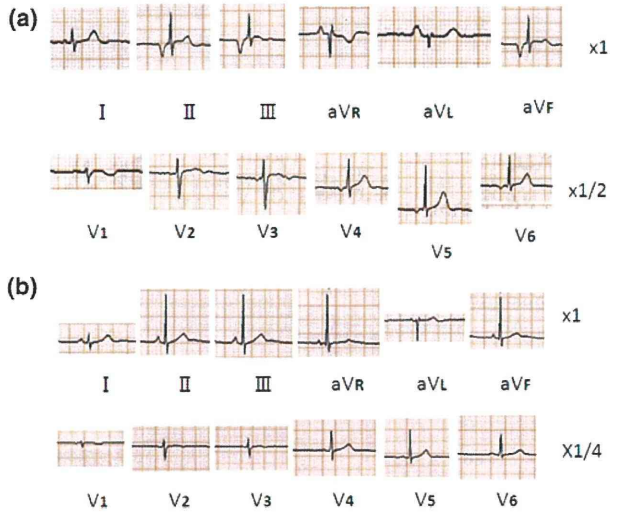

Fig. 1 **a** Before surgery. Negative P waves in *II*, *III*, *aVf*, *V5* and *V6*. **b** 6 months after surgery. Normal P waves with regular rhythm

competitive sport activity [12]. This patient had morphologic characteristics of the anomalous membrane almost identical to those of the reported patient.

In this experience, we performed surgical removal of the anomalous membrane after obtaining an informed consent. Intraoperative direct observation confirmed that the opening was slit-like in shape and located in close proximity to the interatrial septum, with a long axis of 7 mm, which was the same as that measured preoperatively by echocardiography. The operation and the postoperative course were uneventful, and the ECG after the operation showed normal P waves (Fig. 1b).

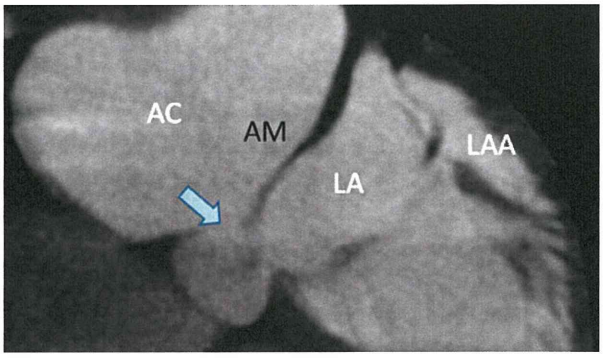

Fig. 3 The anomalous membrane (*AM*) separated the accessory chamber (*AC*) from the left atrium (*LA*). The opening (*arrow*) in the membrane is located along the interatrial septum. *LAA* left atrial appendage

The removed membrane was examined histologically. Hematoxylin-eosin (H&E) staining (Fig. 4a) showed a group of myocardial cells (shown by a star) and two bunches of node-like tissue (shown by yellow arrows). These node-like tissues and the cells around them consisted of cells larger than the working myocardial cells, and their cytoplasm was clear and bright, indicating that these cells were the specialized myocardial cells.

Next, we stained the tissue using Victoria blue-van Gieson (VBG), which indentifies elastic fibers, collagen fibers, and the working myocardial cells. We found that a bunch of clear cells (yellow arrow) was surrounded by fiber tissue and that there were many cells with clear and bright cytoplasm (blue arrows). These portions and cells (indicated by arrows) were negative for the VBG staining,

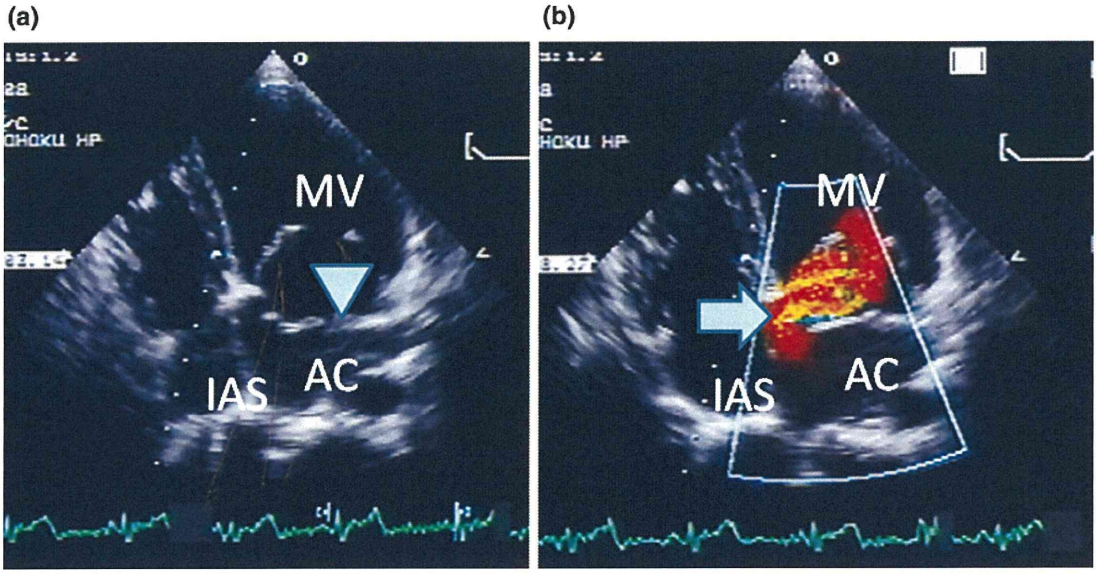

Fig. 2 **a** The anomalous membrane (*inverted triangle*) is visible in 4 chamber view. **b** Color Doppler echocardiogram. Blood stream (*arrow*) from the accessory chamber (*AC*) into the left atrium toward the mitral valve (*MV*) along the interatrial septum (*IAS*)

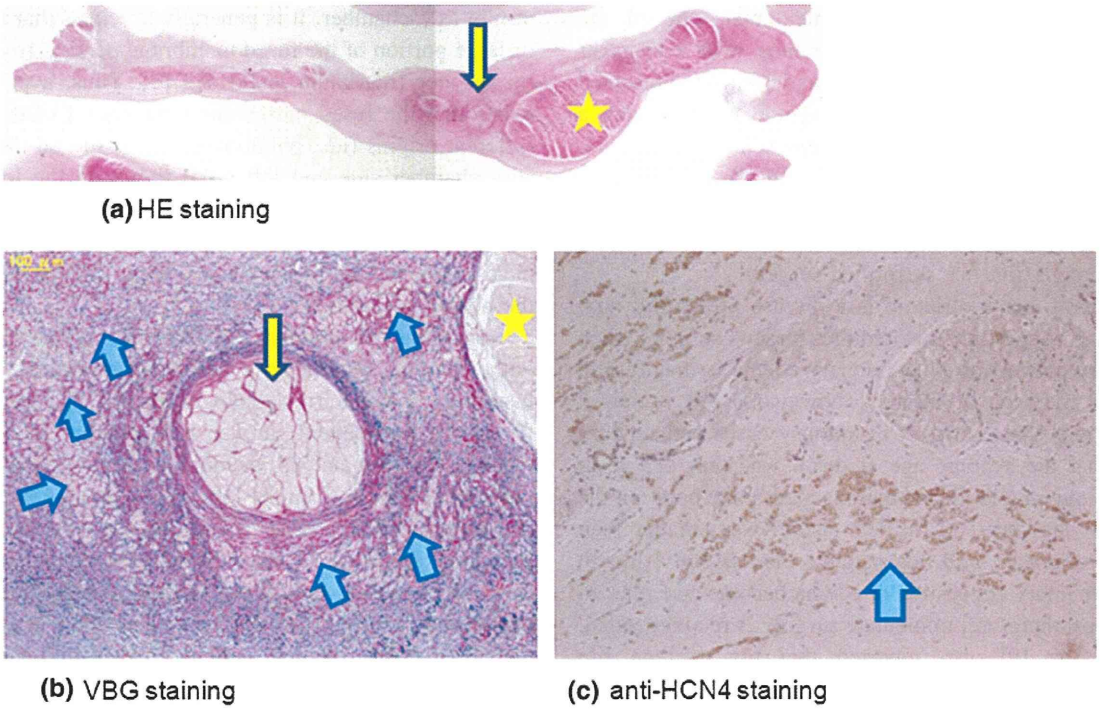

Fig. 4 **a** Hematoxylin-Eosin staining: In the areas (indicated by an *arrow*), there are a bunch of cells, which are larger than the normal myocardial cells and their cytoplasm is bright and clear. The finding indicates that these cells are specialized myocardial cells. The large mass seen at the right part in this section (indicated by a *star*) is a characteristic feature of the working myocardium. **b** Victoria blue-van Gieson (VBG) staining This is magnified figure of the area which is indicated by the *yellow* arrow in **a**. The cells, which were suspected to be specialized myocardial cells by HE staining (*blue arrows*), were not stained by VBG, excluding a possibility that these cells were working myocardial muscle cells, elastic fibers, and/or collagen fibers. And, cells, surrounded by fibers (*yellow arrow*), were also not stained by VBG. **c** Anti-HCN4 antibody staining. This section was almost same as **b**. The HCN-positive cells are those which are presumed by H-E staining to be specialized myocardial cells or cells of the conduction system. This indicates that these cells very likely pose the pacemaker action. *HCN4* hyperpolarization-activated cyclic nucleotide-gated potassium channel 4

indicating that they likely were the specialized myocardial cells.

We then performed immunohistologic staining using antihyperpolarization-activated cyclic nucleotide-gated potassium channel 4 (HCN4) antibody, known to be a marker for the sinoatrial node [1, 8, 10, 11]. The HCN4-positive cells coincided with the cells that seemed to be the specialized myocardial cells by H&E and VBG staining. Thus, we considered that these HCN4 positive cells were the cells of sino-atrial node (SAN) or SAN-like cells, or at least cells with electrical automaticity.

Discussion

Cor triatriatum is relatively rare, occurring at the rate of 0.1–0.4% of all congenital heart disease [3]. This anomaly often presents during infancy, with symptoms and signs caused by pulmonary congestion such as feeding difficulty, poor weight gain, dyspnea, and/or repeated respiratory infections. After infancy, however, cor triatriatum becomes clinically apparent as exertional dyspnea, exercise intolerance or easy fatigability, or even cyanosis with strenuous exercise. However, it may be totally asymptomatic as in our patient, and the diagnosis of asymptomatic patients usually occurs incidentally during an ECG or medical checkup for other reasons.

The diseases presenting with abnormal P wave include heterotaxia syndrome such as polysplenia or left isomerism syndrome [7] and others. Momma et al. [7] investigated the P wave in 50 patients with polysplenia and found a normal P wave in only one patient. Even if the case is not complicated with a hemodynamically significant intracardiac anomaly, polysplenia or left isomerism is known to be associated with sick sinus syndrome or advanced atrioventricular block as patients become older [5]. Thus, to exclude abnormalities associated with the abnormal P waves, we performed echocardiography and as a result found cor triatriatum.

The observed marginal dilation of the pulmonary veins together with the pulmonary wedge pressure at the upper limit of normal range indicated that there was subtle

pulmonary congestion. As we mentioned, one of the authors (M.N.) had previous experience with a teenager who had been completely asymptomatic until he presented suddenly with severe pulmonary edema while playing a badminton game at a tournament representing his school. He underwent emergency surgery, and the morphologic finding was identical to that of the reported case. With this experience and the findings suggestive of the subtle pulmonary congestion, we performed surgery.

In general, cor triatriatum is a disease presenting with pulmonary congestion that requires urgent surgery when pulmonary congestion or pulmonary edema is manifested, which is frequent in infancy. Niwayama [9] reviewed morphologic characteristics in autopsy cases and demonstrated that the average age at death was only 3.3 years when the opening in the anomalous membrane between the accessory chamber and the left atrium was smaller than 3 mm in diameter, and that patients died within 1 month when pulmonary congestion or edema became apparent. In these cases, therefore, immediate surgery is recommended.

Niwayama [9] also reported that the average life expectancy was 16 years if the opening was larger than 3 mm in diameter. The 7-mm opening and the asymptomatic status of our patient seemed to be in accordance with the literature.

The most important and specific point is the presence of electrically active cells in the excised abnormal membrane. We suspected this possibility because the preoperative abnormal P waves were normalized after excision of the membrane. As expected, immunohistologic examination by staining with anti-HCN4 antibody showed a bunch of the staining positive cells in the excised membrane. Reports describe HCN4 staining as a marker of the sinoatrial node in the rat and the rabbit [1, 10, 11]. However, there has been no report on the human, so our result did not definitely confirm that these cells are truly the sinoatrial node cells. However, our finding suggests that the anti-HCN4 antibody positive cells are cells with ability to generate pacemaker action potential in the human even if it is not the sinoatrial node. Moreover, these cells were not stained by VBG, which eliminated the conclusion that they were not elastic fibers, collagen fibers, or working myocardial cells. The results of these two methods suggest that the cell group stained by anti-HCN4 antibody and not by VBG is very likely the sinoatrial node tissue or at least cells with electrical automaticity.

During the early stages of cardiovascular morphogenesis, the common pulmonary vein primordium fuses with the posterior wall of the left atrium. At the beginning, the common pulmonary vein chamber is separated from the left atrium by the fused membrane. Then in the normal process, the fused membrane disappears, causing the common pulmonary vein to be incorporated into the left atrium as a chamber. It is generally accepted that if a part or large portion of the fused membrane persists from some reason, cor triatriatum is formed [4]. Thus, a possibility exists that the fused membrane comprises tissues of two different origins (i.e., pulmonary vein tissue on the accessory chamber side and left atrial tissue on the left atrial side). It is possible that both tissues have cells with pacemaker action. Left atrial rhythm is seen in patients who have congenital heart disease with situs solitus or even in the normal population.

Regarding the pulmonary vein side, the presence of cells with electrical automaticity has been confirmed by both histologic and electrophysiologic studies in recent years [2, 6]. In our patient, it was not possible to ascertain whether the anomalous membrane originated from the pulmonary vein or from the left atrium because the excised tissue appeared as a mass. Therefore, we were not able to ascertain the origin of the cells with pacemaker activity. Regardless of their origin, we showed that the anomalous membrane consisted of cells with pacemaker activity and that the presence of these cells coincided with the anomalous P wave suggestive of left atrial origin, which disappeared after removal of the membrane, resulting in the normal P wave. The reported case showed that the left atrial rhythm or junctional rhythm shown on ECG could be a sign of cor triatriatum.

Acknowledgment The authors acknowledge Drs. Shigehiro Morishima, M.D. and Takashi Ono, M.D. for the operation and Dr Hideo Sakuma, M.D. for the pathologic analysis. This work was supported by an intra-institutional fund.

References

1. Biel M, Schneider A, Wahl C (2002) Cardiac HCN channels: structure, function, and modulation. Trends Cardiovasc Med 12:206–212
2. Chen SA, Hsieh MH, Tai CT et al (1999) Initiation of atrial fibrillation by ectopic beats originating from the pulmonary veins: electrophysiological characteristics, pharmacological responses, and effects of radiofrequency ablation. Circulation 18:1879–1886
3. Geva T, Van Praagh S (2008) Anomalies of the pulmonary veins. In: Allen HD, Driscoll DJ, Shaddy RE, Feltes TF (eds) Moss and Adams' heart disease in infants Children and adolescents. Wolters Kluwer/Lippincott Williams & Wilkins, Philadelphia, pp 761–792
4. Gharagozloo F, Bulkley BH, Hutchins GM (1977) A proposed pathogenesis of cor triatriatum. Am Heart J 94:618–626
5. Gilljam T, Freedom RM, Yoo SJ (2004) The syndrome of isomeric left atrial appendages, often associated with polysplenia. In: Freedom RM, Yoo SJ, Mikailian HJ, Williams WG (eds) The natural and modified history of congenital heart disease. Blackwell, Oxford, pp 430–434
6. Haissaguerre M, Jais P, Shah DC et al (1998) Spontaneous initiation of atrial fibrillation by ectopic beats originating in the pulmonary veins. N Engl J Med 10:659–666

7. Momma K, Takao A, Shibata T (1990) Characteristics and natural history of abnormal atrial rhythms in left isomerism. Am J Cardiol 65:231–236
8. Moosmang S, Stieber J, Zong X et al (2001) Cellular expression and functional characterization of four hyperpolarization-activated channels in cardiac and neuronal tissues. Eur J Biochem 268:1646–1652
9. Niwayama G (1960) Cor triatriatum. Am Heart J 59:291–317
10. Shi W, Wymore R, Yu H et al (2002) Distribution and prevalence of hyperpolarization-activated cation channels (HCN) mRNA expression in cardiac tissues. Circ Res 85:e1–e6
11. Stieber J, Herrmann S, Feil S et al (2003) The hyperpolarization-activated channel HCN4 is required for the generation of pacemaker action potentials in the embryonic heart. Proc Natl Acad Sci USA 215:15235–15240
12. Uemura M, Nishibatake N, Nakazawa M et al (1988) Clinical aspect of cor triatriatum. Acta Paediatr Japonica 92:1294–1300

Arteriosclerosis, Thrombosis, and Vascular Biology

JOURNAL OF THE AMERICAN HEART ASSOCIATION

Xanthine Oxidoreductase Is Involved in Macrophage Foam Cell Formation and Atherosclerosis Development

Akifumi Kushiyama, Hirofumi Okubo, Hideyuki Sakoda, Takako Kikuchi, Midori Fujishiro, Hirokazu Sato, Sakura Kushiyama, Misaki Iwashita, Fusanori Nishimura, Toshiaki Fukushima, Yusuke Nakatsu, Hideaki Kamata, Shoji Kawazu, Yukihito Higashi, Hiroki Kurihara and Tomoichiro Asano

Arterioscler Thromb Vasc Biol. 2012;32:291-298; originally published online November 17, 2011;
doi: 10.1161/ATVBAHA.111.234559
Arteriosclerosis, Thrombosis, and Vascular Biology is published by the American Heart Association, 7272 Greenville Avenue, Dallas, TX 75231

Print ISSN: 1079-5642. Online ISSN: 1524-4636

Xanthine Oxidoreductase Is Involved in Macrophage Foam Cell Formation and Atherosclerosis Development

Akifumi Kushiyama, Hirofumi Okubo, Hideyuki Sakoda, Takako Kikuchi, Midori Fujishiro, Hirokazu Sato, Sakura Kushiyama, Misaki Iwashita, Fusanori Nishimura, Toshiaki Fukushima, Yusuke Nakatsu, Hideaki Kamata, Shoji Kawazu, Yukihito Higashi, Hiroki Kurihara, Tomoichiro Asano

Objective—Hyperuricemia is common in patients with metabolic syndrome. We investigated the role of xanthine oxidoreductase (XOR) in atherosclerosis development, and the effects of the XOR inhibitor allopurinol on this process.

Methods and Results—Oral administration of allopurinol to ApoE knockout mice markedly ameliorated lipid accumulation and calcification in the aorta and aortic root. In addition, allopurinol treatment or siRNA-mediated gene knockdown of XOR suppressed transformation of J774.1 murine macrophage cells, treated with acetylated LDL or very low density lipoprotein (VLDL) into foam cells. This inhibitory effect of allopurinol was also observed in primary cultured human macrophages. In contrast, overexpression of XOR promoted transformation of J774.1 cells into foam cells. Interestingly, SR-A1, SR-B1, SR-B II, and VLDL receptors in J774.1 cells were reduced by XOR knockdown, and increased by XOR overexpression. Conversely, expressions of ABCA1 and ABCG1 were increased by XOR knockdown and suppressed by XOR overexpression. Finally, productions of inflammatory cytokines accompanied by foam cell formation were also reduced by allopurinol administration.

Conclusion—These results strongly suggest XOR activity and/or its expression level to contribute to macrophage foam cell formation. Thus, XOR inhibitors may be useful for preventing atherosclerosis. **(*Arterioscler Thromb Vasc Biol.* 2012; 32:291-298.)**

Key Words: atherosclerosis ■ cell physiology ■ cytokines ■ macrophages ■ xanthine oxidoreductase

A relationship between serum uric acid levels and atherosclerotic disease development has been suggested.[1–3] In addition, there is epidemiological evidence of an association between hyperuricemia and metabolic syndrome,[1] type 2 diabetes,[4] chronic kidney diseases,[5,6] heart failure incidence in older adults,[7] and with mortality in patients undergoing percutaneous coronary intervention or with acute myocardial infarction.[8–10] Uric acid itself reportedly functions as an antioxidant,[11] though the process of uric acid synthesis is accompanied by the generation of reactive oxygen species.

Xanthine oxidoreductase (XOR) is a key enzyme in the uric acid production pathway; XOR oxidizes hypoxanthine from nucleic acid metabolites into xanthine, and xanthine into uric acid. XOR basically oxidizes a variety of purines and pterins, classified as molybdenum iron-sulfur flavin hydroxylases. XOR tissue and cellular distributions are high in the mammalian liver and intestine due to XOR-rich parenchymal cells.[12] XOR activity is low in human serum, brain, heart, and skeletal muscle, though a recent study revealed microvascular endothelial cells to be rich in XOR activity.[13] It seems that XOR does not induce harmful reactive oxygen species production under normal conditions but in pathological states such as ischemic congestive heart failure, XOR activity increases drastically and XOR localizes within CD68 positive macrophages.[14] Allopurinol, a xanthine oxidase (XO) inhibitor, has been widely used for hyperuricemia treatment. Oxypurinol, a hydroxide and the main metabolite of allopurinol generated by XOR, covalently binds to XOR and thereby inhibits its activity.[15] Allopurinol reportedly ameliorates chronic stable angina[16] and protects the heart during ischemic reperfusion,[17] and oxypurinol improves the left ventricular ejection fraction in congestive heart failure patients with low left ventricular ejection fraction.[18] It was also suggested that XO inhibitors improve endothelium-dependent vascular relaxation in blood vessels of hyperlipidemic rabbits.[19]

Macrophages play key roles in atherosclerosis development. Macrophages migrate into pathological lesions such as dysfunctional endothelium and then develop into foam cells,

Received on: July 12, 2011; final version accepted on: November 7, 2011.

From the Department of Metabolic Diseases (A.K., T.K., H.S., S.K.), The Institute for Adult Diseases, Asahi Life Foundation, Tokyo, Japan; Department of Medical Chemistry (H.O., M.I., F.N., T.F., Y.N., H.K., Y.H., T.A.), Division of Molecular Medical Science, Graduate School of Biomedical Sciences, Hiroshima University, Hiroshima, Japan; Department of Internal Medicine (H.S., M.F.), Graduate School of Medicine, University of Tokyo, Tokyo, Japan; Department of Physiological Chemistry and Metabolism (S.K., H.K.), Graduate School of Medicine, The University of Tokyo, Tokyo, Japan.

Akifumi Kushiyama and Hirofumi Okubo contributed equally to this study.

Correspondence to Tomoichiro Asano, 1-2-3 Kasumi, Minami-ku, Hiroshima, 734-8553, Japan. E-mail asano-tky@umin.ac.jp

Arterioscler Thromb Vasc Biol **is available at http://atvb.ahajournals.org** **DOI: 10.1161/ATVBAHA.111.234559**

which contribute to vascular stenosis and plaque instability. Foam cell formation by macrophages is accelerated by several extracellular factors, ie, LDL, especially modified LDL,[20] such as oxidized LDL or acetyl LDL (AcLDL), very low density lipoprotein (VLDL),[21] and saturated free fatty acids, as well as by cellular mechanisms such as lipid uptake, metabolism, and efflux. The serum of Watanabe heritable hyperlipidemic rabbits (WHHL), characterized by a mutated LDL receptor, also reportedly induces macrophage foam cell formation.[22,23] Moreover, foam cells secrete cytokines such as tumor necrosis factor (TNF)-α, interleukin (IL)-6 and IL-1β,[24] inducing cellular migration and apoptosis, which also contribute to the development of unstable plaques. The relationships between uric acid metabolism and atherosclerosis and their underlying mechanisms have yet to be elucidated. We thus investigated the effects of XOR and an inhibitor, allopurinol, on atherosclerosis development, focusing especially on effects on macrophages.

Materials and Methods

Animals

This study was approved by the Ethics Committee of the Institute for Adult Diseases, Asahi Life Foundation. All animal experiments were conducted in accordance with the Guidelines for the Care and Use of Laboratory Animals of the same institution. ApoE knockout (KO) mice (B6.129P2-Apoe^{tm1Unc}/J) were purchased from Charles River Co. (Wilmington, MA). All mice were maintained under pathogen-free conditions and a 12-hour light/dark cycle with free access to food and water. The 9-month-old ApoE KO mice were given water either with or without 10 μmol/L allopurinol for 4 weeks, as previously described.[25] The water was replaced every 2 days. Food was withdrawn 12 hours before the experiment.

Preparation of Tissue Samples for Histological Analysis

Nine-month-old mice, with and without allopurinol administration, were euthanized. The heart and entire aorta were removed en bloc and then formalin-fixed. Samples were rinsed with phosphate-buffered saline and aortic roots were routinely embedded in OTC compound (Sakura Finetek Japan, Tokyo, Japan). Sequential 5-μm slices of the aortic root were obtained. The aortic tree was incised longitudinally and then rinsed with phosphate-buffered saline.

Histological Analysis

The aortic root slices and opened aortic trees were stained with oil red O, as previously described.[26] Aortic root slides were counterstained with hematoxylin. In addition, these samples were processed for immunofluorescent staining with antimacrophage antibody (Ab) (1:200, Abcam #56297, Cambridge, UK), and Alexa-fluor488-labeled anti-rat IgG (1:250, Invitrogen, CA). DAPI staining was used to detect the nuclei. Digital images of lesions were obtained with a Nikon Eclipse 50 microscope.

Areas of calcification and lipid accumulation as well as those of macrophage accumulation were histomorphometrically analyzed using MultiGauge ver. 3.1 (FujiFilm, Tokyo, Japan), according to the manufacturer's instructions. The ratios of the lesion area stained by oil red O and that of macrophage accumulation, to the whole aortic wall area and the arterial wall area, respectively, were calculated. In addition, the ratios of calcified or lipid accumulation areas to the whole aortic wall surface were similarly calculated.

Serum Investigation

Serum triglyceride (TG), cholesterol, free fatty acids, and uric acid were assayed with the Triglyceride E test, Cholesterol E test, HDL Cholesterol E test, NEFA C test, and UA C test (all from Wako Chemicals, Osaka, Japan), respectively, according to the manufacturer's instructions. LDL cholesterol (cLDL) was calculated by the Friedewald formula as previously described.[27]

Reagents and Cell Culture

The murine macrophage J774.1 cell line was purchased from Riken (Tsukuba, Japan), cultured in RPMI 1640 (Sigma-Aldrich, St. Louis, MO) medium supplemented with 10% fetal calf serum (Invitrogen), penicillin 100 U/mL, and streptomycin 100 μg/mL (Invitrogen) at 37°C in 5% CO_2. Allopurinol and all reagents were of analytic grade. Lipopolysaccharide (LPS) from Escherichia coli 0111: B4 was purchased from Sigma-Aldrich Japan. Serum of 3-month-old WHHL rabbits was purchased from Oriental Yeast (Tokyo, Japan). Primary Ab for western blotting and immuno-fluorescent staining were purchased, as follows: anti-XOR (Santa Cruz Biotechnology, CA, #sc-20991), LDLR (Cayman Chemical, MI, #1007665), VLDL receptors, SR-A1 (R&D Systems, MN, #AF2258, 1797), CD36 (Lifespan Bioscience, WA, #LS-B662/10019), SR-B1, -B2, ABCG1 (Novus Biologicals, CO, #NB400–101, 102, 132) and ABCA1 (Thermo Scientific, MA, #PA1-16789).

Isolation and Purification of Primary Human Macrophages

To obtain monocytes/macrophages, we isolated peripheral blood mononuclear cells were isolated from 20 mL of blood by centrifugation over a density gradient using Ficoll-Paque PREMIUM (GE Healthcare Japan, Tokyo, Japan). Peripheral blood mononuclear cells were resuspended in 10 mL of RPMI 1640 medium containing 10% fetal bovine serum and purified using MSP-P (JIMRO, Gunma, Japan) according to the manufacturer's instructions. The primary human macrophages obtained were spread onto 24-well culture plates. The indicated concentration of allopurinol was added to the medium 2 hours prior to additional incubation with 50 μg/mL AcLDL (COSMO-Bio, Tokyo, Japan) for 24 hours. After incubation with or without allopurinol or AcLDL, the cells were stained with AdipoRed according to the manufacturer's instructions. Lipid accumulation in macrophages was visualized with a Leica DMIRB microscope.

Quantification of Lipid Accumulation in Macrophages

J774.1 cells were cultured at 90% confluence on 96-well or 12-well plates for lipid accumulation assays as previously described.[28] The indicated concentration of allopurinol was added to the medium 2 hours prior to additional incubation with 10 ng/mL LPS, 1% WHHL rabbit serum, 50 μg/mL AcLDL or 50 μg/mL VLDL, for 24 hours. The cells were then stained with AdipoRed and visualized with a Leica DMIRB microscope, or subjected to lipid accumulation quantification using an ARVO MX fluorimeter (PerkinElmer, MA), according to the manufacturer's instructions.

DiI AcLDL Uptake Assay

For the DiI (3,3′-dioctadecylindocarbocyanine)-AcLDL uptake assay, 50 μg/dL DiI AcLDL were added to RPMI 1640 medium containing the indicated concentrations of WHHL rabbit serum and allopurinol. Then the cells were incubated for another 4 hours, and finally rinsed twice with phosphate-buffered saline. Cellular DiI-AcLDL uptake was then measured using the ARVO MX fluorimeter.

Overexpression of XOR and Knockdown of XOR

The cDNA encoding mouse XOR was obtained from Kazusa DNA Research Institute (Chiba, Japan). XOR cDNA and control LacZ cDNA were each inserted into pcDNA3.1(+) plasmids. The siRNAs of XOR and the control were purchased from Invitrogen (XOR siRNA #1320003 MSS238717, control siRNA HiGC 12935-400). Lipofection of cDNA plasmids or siRNA was performed using FuGene HD (Roche, Basel, Switzerland) or lipofectamine RNAiMAX (Invitrogen), respectively, according to the manufacturer's instructions.

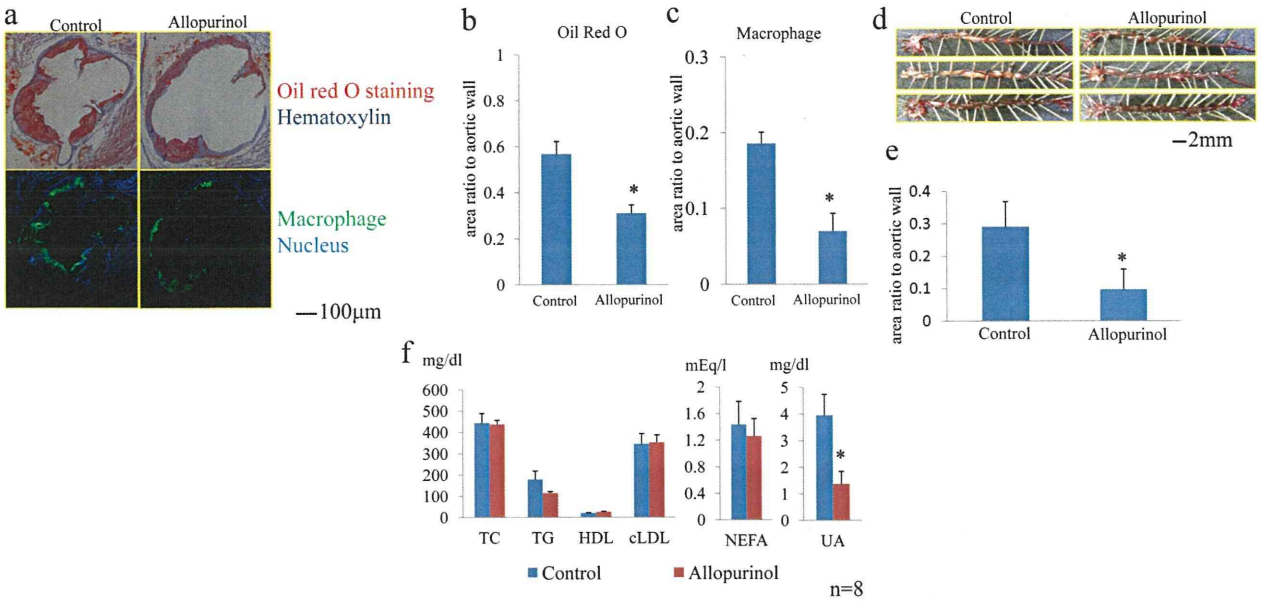

Figure 1. The in vivo effect of allopurinol against atherosclerotic lesion development. **a**, Oil red O staining and macrophage immunostaining of the aortic roots of 9-month-old ApoE knockout (KO) mice with and without allopurinol administration. Upper panels show Oil Red O staining and counterstaining with hematoxylin. Lower panels show macrophage immunostaining (**Green**) and counterstaining with DAPI (**Blue**). **b**, Quantification of lesion area, stained with Oil Red O. Mean±SE. The ratio of the stained lipid area to the arterial wall area is presented. **c**, Quantification of immunostained macrophage area. Mean±SE. The ratio of the stained macrophage area to the arterial wall area is presented. **d**, Oil red staining of incised aortic wall throughout the aortic tree. Lipid accumulation including the area of calcification is stained orange. **e**, Quantification of lesion area, stained with Oil Red O. Mean±SE. The ratio of the stained lipid and calcified area to the arterial wall inner surface is presented. **f**, Serum examinations of ApoEKO mice with and without allopurinol administration. cLDL indicates calculated LDL; TC, total cholesterol; TG, triglyceride; NEFA, non-esterified fatty acid; UA, uric acid. The asterisk (*) indicates statistical significance at $P<0.05$.

Western Blotting

Western blot analysis was carried out as described previously.[29] In brief, 10 μg of protein were separated by SDS-PAGE and electrophoretically transferred to membranes, which were then incubated with specific Ab. The antigen-Ab interactions were visualized using HRP-conjugated secondary Ab and SuperSignal West Pico Chemiluminescent Substrate (Thermo Scientific). Band images were obtained with LAS-4000 (FujiFilm) and quantified using MultiGauge ver. 3.1. Fold changes in protein expressions, as compared to β-actin, were determined in triplicate.

Quantification of Cytokine Expressions

J774.1 cells were cultured in RPMI 1640 with 10% FCS. The indicated concentration of allopurinol was added to the medium 2 hours prior to additional incubation with 10 ng/mL LPS or 1% WHHL rabbit serum for 24 hours. Then, mRNA was prepared from the cells using an RNeasy-mini kit (QIAGEN, Hilden, Germany) according to the manufacturer's instructions and 1 μg of this mRNA was reverse transcribed with Transcriptor Reverse Transcriptase (Roche). Quantitative real-time PCR was run with a LightCycler480 (Roche Diagnosis Japan) using FastStart SYBR Green Master (Roche). The primers were designed as follows: mouse IL-1β forward, 5′-TCGCTCAGGGTCACAAGAAA-3′, mouse IL-1β reverse, 5′-CATCAGAGGCAAGGAGGAAAAC-3′, mouse IL-6 forward, 5′-GATGCTACCAAACTGGATATAATC-3′, mouse IL-6 reverse, 5′-CTGGCACCACTAGTTGGTTGTC-3′, mouse TNF-α forward, 5′-GCCACCACGCTCTTCTGTCT-3′, mouse TNF-α reverse, 5′-GTCTGGGCCATAGAACTGAT-3′, mouse actin forward, 5′-ATCATTGCTCTCCTGAGCG-3′, mouse actin reverse, 5′-GCTGATCCACATCTGGAA-3′. Post-PCR melting curves confirmed the specificity of single-target amplification. Relative gene expressions were calculated by the efficiency correction method.[30] Fold changes in the expressions of IL-1β, IL-6, IL-12, and TNF-α normalized by the actin level were determined in triplicate.

Statistical Analysis

Results are presented as means±SE. ANOVA and Student *t* test were used for parametric data, the Mann-Whitney U test for nonparametric data. Statistical significance was $P<0.05$.

Results

In Vivo Quantification of Atherosclerotic Plaque in ApoE KO Mice

A 10 μmol/L dose of allopurinol was administered daily for 4 weeks to 9-month-old ApoE KO mice (n=8). Oil red O staining revealed markedly reduced lipid accumulation in the aortic roots of allopurinol-treated ApoE KO mice (upper panels of Figure 1a), quantified as a 45.5% reduction in lipid droplets as compared with control ApoE KO mice (Figure 1b). Numbers of macrophages in aortic sections were also significantly lower, as shown by immunostaining (lower panels of Figure 1a), and quantification revealed a 72.2% reduction in the macrophage accumulation area (Figure 1c). The area of calcification in the aorta (Figure 1d) was also estimated and revealed a 67.0% reduction in the allopurinol-treated group, as compared with the control (Figure 1e). In allopurinol-treated mice, serum TG levels were slightly lower than in control mice, but this difference was not statistically significant (Figure 1f). Serum uric acid was reduced by 65.1%, whereas serum concentrations of total cholesterol, HDL, cLDL, and free fatty acids did not differ between the allopurinol-treated and control groups (1f). There were no differences in body weight between the 2 groups throughout the study period

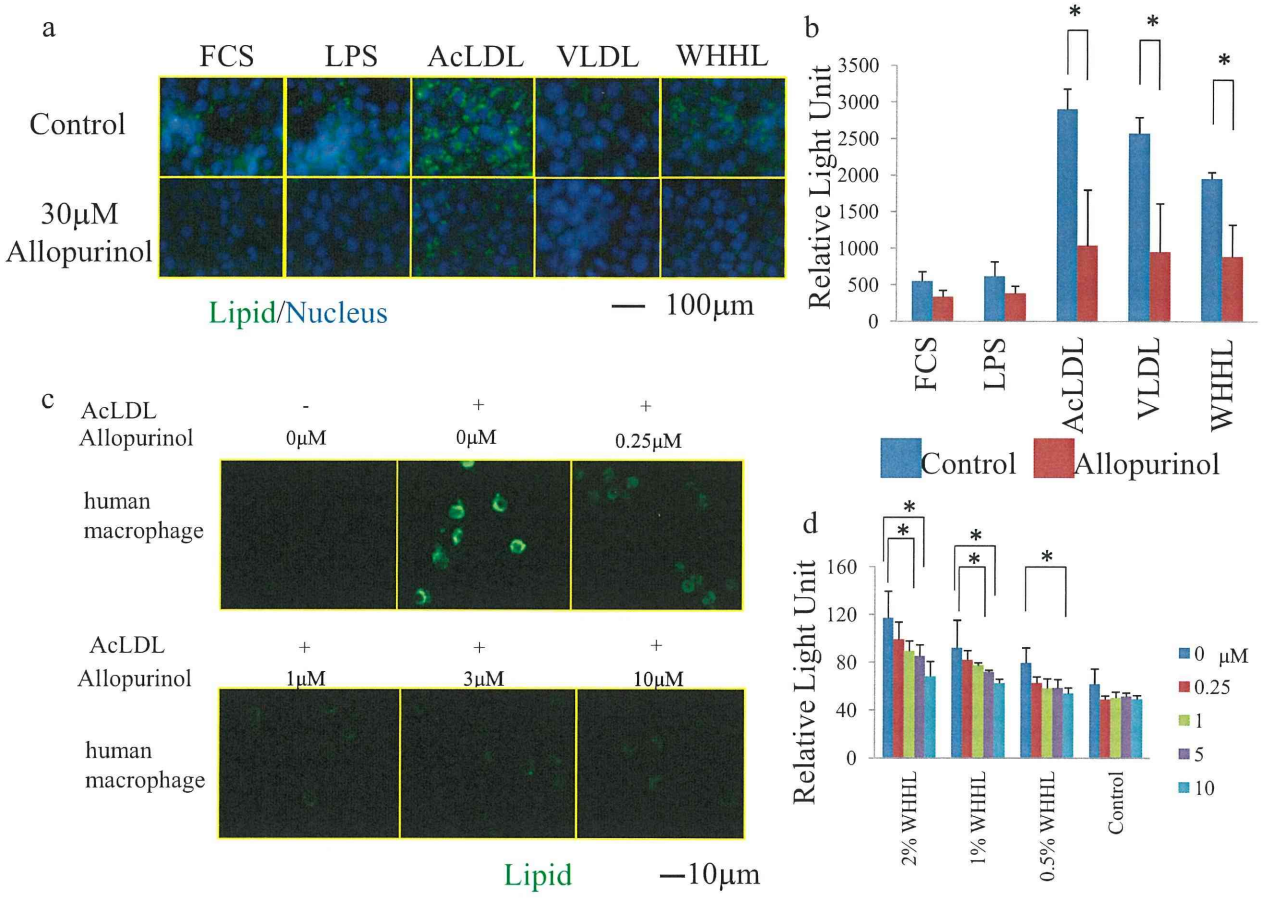

Figure 2. Lipid accumulation within J774.1 cells and human isolated macrophages. **a**, AdipoRed staining was performed and lipid accumulation was quantified. The effects of 30 μmol/L allopurinol on lipid accumulation in J774.1 cells induced by 10 ng/mL LPS, 50 μg/mL acetyl LDL (AcLDL), 50 μg/dL VLDL, and 1% WHHL rabbit serum are shown. Cellular lipid is stained green by AdipoRed, the nucleus is stained blue by DAPI. **b**, Quantification of cellular lipids stained by AdipoRed, induced as in 2a. The asterisk (*) indicates statistical significance at $P<0.05$. **c**, AdipoRed staining was performed on human isolated macrophages treated with 50 μg/mL AcLDL for 24 hours. The indicated concentration of allopurinol was added 2 hours prior to AcLDL incubation. Cellular lipid is stained green by AdipoRed. **d**, Assay of DiI AcLDL uptake. The effect of allopurinol administration on AcLDL uptake was quantified. LPS indicates lipopolysaccharide; VLDL, very low density lipoprotein; WHHL, Watanabe heritable hyperlipidemic rabbits.

(data not shown). Thus, allopurinol markedly suppressed atherosclerosis in vivo without significantly altering cholesterol levels.

In Vitro Quantification of Macrophage Foam Cell Formation

J774.1 cells were incubated with 10 ng/mL LPS, 50 μg/mL AcLDL, 50 μg/mL VLDL, or 1% WHHL rabbit serum in the absence or presence of the indicated allopurinol concentrations (Figure 2a and 2b). Transformation of J774.1 cells into lipid-containing foam cells was examined by Adipored staining, followed by quantification. It was revealed that allopurinol reduced lipid accumulation in J774.1 cells, induced by AcLDL, VLDL, or WHHL rabbit serum. LPS treatment for 24 hours did not affect lipid accumulation in J774.1 cells. Very similarly, allopurinol markedly ameliorated AcLDL-induced lipid accumulation in primary human macrophages (Figure 2c).

Allopurinol Suppresses Uptake of AcLDL Into Macrophages

Because AcLDL-induced transformation of J774.1 cells into foam cells was suppressed, the effect of allopurinol on AcLDL uptake was investigated. The J774.1 cells were incubated with normal or 0.5% to 2% WHHL rabbit serum, in the absence or presence of the indicated allopurinol concentrations. Then, transport of DiI AcLDL into the cells was examined. Allopurinol concentration-dependently inhibited WHHL serum-enhanced DiI AcLDL uptake, but had no effect on that taken up by cells incubated with normal rabbit serum (Figure 2c).

XOR Expression and Lipid Accumulation

Because allopurinol was shown to inhibit lipid accumulation in macrophages, we next examined the effect of XOR overexpression, which resulted in an approximately 1.8-fold increase in total expression of XOR protein, whereas siRNA-mediated gene-knockdown of XOR resulted in a 50% expression reduction (Figure 3a). XOR overexpression exacerbated foam cell formation (Figure 3b and 3c) and increased DiI-AcLDL uptake (Figure 3d) into J774.1 cells, although these reactions were inhibited by XOR knockdown (Figure 3b, 3e, and 3f). XOR overexpression also induced lipid accumulation even in the absence of additional lipids in the medium.